Article

Nitric oxide activates #-cell glucokinase by promoting formation of the 'glucose-activated' state.

Kendra Seckinger, Vishnu P. Rao, Nicole E. Snell, Allison E Mancini, Michele L. Markwardt, and M A Rizzo

Biochemistry, **Just Accepted Manuscript** • DOI: 10.1021/acs.biochem.8b00333 • Publication Date (Web): 27 Jul 2018

Nitric oxide activates β-cell glucokinase by promoting formation of the 'glucose-activated' state.

Kendra M. Seckinger, Vishnu P. Rao, Nicole E. Snell, Allison E. Mancini, Michele L. Markwardt, and M. A. Rizzo[1]

Department of Physiology, University of Maryland School of Medicine, Baltimore, Maryland 21201

Running title: *NO-mediated GCK activation in cells.*

[1]Address correspondence to M. A. Rizzo, Ph.D., 660 W. Redwood St., HH 525B, Baltimore, MD, 21201. Phone: (410) 706-2421; Fax: (410) 706-8341; E-mail: mrizzo@som.umaryland.edu

Keywords: FRET, glucokinase, nitric oxide, diabetes, MODY, homotransfer

This work was funded by NIH grants R01DK077140 and R01MH111527 to M.A.R. and NIH Training grants T32GM008181 and T32DK098107 for support of K.M.S.

Abstract

Insulin release from the pancreas is tightly controlled by glucokinase (GCK) activity which couples β-cell metabolism to changes in blood sugar. Despite only having a single glucose-binding site, GCK displays positive glucose cooperativity. *Ex vivo* structural studies have identified several potential protein conformations with varying levels of enzymatic activity, yet it is unclear how living cells regulate GCK cooperativity. To better understand the cellular regulation of GCK activation, we developed a homotransfer FRET–GCK biosensor and used polarization microscopy to eliminate fluorescence crosstalk from FRET quantification and improve the signal-to-noise ratio. This approach enhanced sensor contrast compared to the heterotransfer FRET–GCK reporter and allowed observation of individual GCK states using an automated method to analyze FRET data at the pixel level. Mutations known to activate and inhibit GCK activity produced distinct anisotropy distributions, suggesting that at least two conformational states exist in living cells. High glucose activated the biosensor in a manner consistent with GCK's enzymology. Interestingly, glucose-free conditions did not affect GCK biosensor FRET, indicating that there is a single low-activity state, counter to proposed structural models of GCK cooperativity. Under low glucose conditions, application of chemical NO donors efficiently shifted GCK to the more active conformation. Notably, GCK activation by mutation, high glucose, a pharmacological GCK activator, or S-nitrosylation all shared the same FRET distribution. These data suggest a simplified model for GCK activation in living cells, where post-translational modification of GCK by S-nitrosylation facilitates a single conformational transition that enhances GCK enzymatic activity.

Introduction

Glucokinase (GCK) sets the rate of glucose metabolism in the pancreatic β-cell, making it the primary controller of glucose-stimulated insulin secretion. Resting blood sugar levels are therefore quantitatively tied to GCK activity (*1*), and mutations that alter the ability of GCK to phosphorylate glucose are associated with human diseases. Notably, deactivating human GCK mutations cause Type 2 maturity-onset diabetes of the young (MODY2), and activating mutations are linked to clinical hyperinsulinemia (*2*, *3*).

GCK activity shows positive cooperativity for glucose dependence, which is thought to facilitate the metabolism of rising blood glucose levels in the β-cell (*4*, *5*). Simulations of glucose-stimulated insulin secretion have shown that the ATP/ADP ratio is most steeply coupled to glucose concentrations in the 5-10 mM range, past the inflection point for GCK cooperativity, before plateauing above 10 mM glucose (*6*). Given that an increase in the ATP/ADP ratio drives closure of the ATP-dependent K^+ channels leading to glucose-initiated action potentials and insulin secretion, the specific activity of GCK at 5-10 mM glucose concentrations is critical for the β-cell secretory response to the post-prandial rise in glucose (*7*).

The mechanism underlying glucose-dependent changes in GCK activity is atypical. GCK has only a single glucose binding site (*8*), and regulation of the conformational change underlying its allostericity is thought to be primarily kinetic (*9*). The GCK structure consists of two globular domains with the active site residing in the cleft between the two lobes (*10*, *11*). In the absence of glucose, the small domain has been shown to unfold partially into a 'super-open' conformation. Glucose binding stabilizes folding of the small domain in an 'open' state. Once bound, a second conformational change can occur where the structure clamps around glucose. The activated 'closed' state is transient, but can be stabilized in sufficiently high glucose concentrations and can also promote the association of a replacement substrate quickly after the release of glucose-6-phosphate but before GCK can relax to the 'open' conformation (*12*).

While the sequence of events that contribute to the glucose allosteric trait has been studied using *ex vivo* NMR and X-ray crystallography, important questions remain about GCK activation in a physiologic context. First, the extent that each of the three identified GCK conformations exists in nature is unclear, where the range of glucose levels is far narrower (4-8 mM) than the experimental conditions (0-200 mM) (*12*) used to identify the different GCK states. Second, cellular regulation of GCK activity can involve post-translational regulation through protein-protein interactions (*13–15*) or modifications such as S-nitrosylation of Cys371

by nitric oxide (NO) (*15*). It is unknown how these cellular regulatory mechanisms affect known GCK conformational states or whether they induce entirely new ones.

To reconcile the biochemical studies with cellular models of GCK regulation, we developed a homotransfer Förster resonance energy transfer (FRET) GCK biosensor and used quantitative analyses to measure steady-state conformational changes in living cells. This methodology was then used to examine the number of detectable GCK conformational states in living β-cells under various conditions. Our findings suggest a mechanism underlying physiologic activation of GCK by glucose and NO in pancreatic β-cells.

Materials and Methods

Reagents –DNA preparation kits were from Qiagen. DNA primers were from Integrated DNA Technologies. Chemicals were from Sigma-Aldrich unless otherwise noted.

Cell Culture – βTC3 cells (*16*) were cultured in DMEM growth media supplemented with 4.5 g/L glucose, L-glutamine (Cellgro), 10% horse serum (ThermoFisher), 2.5% fetal bovine serum (Invitrogen), and 1% penicillin-streptomycin solution (HyClone). Cells were incubated at 37°C with 5% CO_2. For experiments, cells were seeded on 35 mm dishes containing No. 1.5 glass coverslips (MatTek). Transfections were performed using LipoD293 from SignaGen Laboratories according to the manufacturer's instructions. Experiments were performed 48–72 h post-transfection.

Vector preparation – The mCerulean fluorescent protein (FP) in a previous two-color FRET sensor (*17*) was replaced with an mVenus FP using NheI and BglII restriction sites to create the homotransfer FRET–GCK reporter. Point mutagenesis utilized the QuikChange method (Agilent) with the following primers; GCK(A456V) – sense (5'-GGTCTCTGCGGTGGTCTGCAAGAAGGCTT-3'; antisense, 5'-AAGCCTTCTTGCAGACCACCGCAGAGACC-3'), GCK(K414E) – sense (5'-CTCGGGTGCAGCTCGTACACGGAGCCA-3'; antisense, 5'-TGGCTCCGTGTACGAGCTGCACCCGAG-3'). The mVenus tandem dimer was constructed by removing GCK from the FRET–GCK sensor using the BglII and BamHI restriction sites. The two mVenus FPs were ligated with a ten amino acid linker sequence (SGLRSPPVAT) remaining between them. DNA sequencing (Genewiz, South Plainfield, NJ) was used to verify successful construction of all sensors.

Fluorescence Microscopy – Transfected βTC3 cells were incubated in serum-free imaging media (125 mM NaCl, 5.7 mM KCl, 2.5 mM $CaCl_2$, 1.2 mM $MgCl_2$, 10 mM HEPES, 2 mM glucose, 0.1% bovine serum albumin, pH 7.4) for 3 h before imaging. Images were collected using a Zeiss AxioObserver microscope equipped with a 20×, 0.75 NA Plan-Apochromat objective. For heterotransfer experiments, cells were excited with a 455 nm LED and a T455LP filter cube (Zeiss). CFP and YFP emitted light were separated by a Dual-View (Optical Insights) containing the CFP and YFP filter sets. For the homotransfer experiments, cells were excited using polarized 505 nm light and a 46 HE YFP filter cube. Parallel (*P*) and perpendicularly (*S*) oriented emitted photons were separated by a Dual-View (Optical Insights) containing the polarization filter set (*18–20*). Images were collected at 37°C using a Zeiss incubation system with a water-cooled Hamamatsu C10600 Orca R2 camera. Curve fitting and statistical analysis were performed using GraphPad Prism software.

Ratio FRET images – Ratio images were generated from image data collected using a 20×, 0.75 NA objective and a 1.6× optovar for additional magnification. Images were smoothed before background subtraction and image division using FIJI software (*21*). For clarity, a threshold mask was applied to exclude non-cellular regions.

Calculation of pixel anisotropy (r) values – Dual-View images containing parallel (*P*) and perpendicular (*S*) fluorescence were separated into their component images and aligned by batch processing in FIJI. Images were then processed using R statistical computing language (https://www.r-project.org) and the Bioconductor EBImage analysis package (*22*). Pixels from cells were separated from the background using pixel intensity values as selection criteria. Anisotropy values were calculated for each pixel using the following equation: $(P - gS)/(P + 2gS)$, where g corrects for the polarization bias of the instrument (*18*). Pixels containing an insufficient signal or approaching saturation were excluded from the analysis.

Results

Homotransfer FRET–GCK sensor

We have previously used heterotransfer FRET biosensors to examine GCK activation in living cells (*15*, *17*, *23–26*). Even so, the two-color approach has inherent disadvantages, including low signal-to-noise (*27*) and spectral overlap (*28*, *29*), that can be circumvented using a

homotransfer approach. Therefore, we converted a two-color FRET–GCK sensor (*17*) to a homotransfer reporter by replacing the cyan FRET donor with a second mVenus fluorescent protein (FP). The resulting sensor contains two mVenus FPs at the N- and C-termini of GCK (Fig. 1A).

βTC3 insulinoma cells were transiently transfected with either FRET sensor and incubated in low glucose conditions for 3 h before image collection by fluorescence microscopy. Addition of exendin-4, a glucagon-like peptide-1 receptor agonist, was used to stimulate GCK activation (*17*, *30*, *31*). The ratio of acceptor to donor fluorescence under CFP illumination was

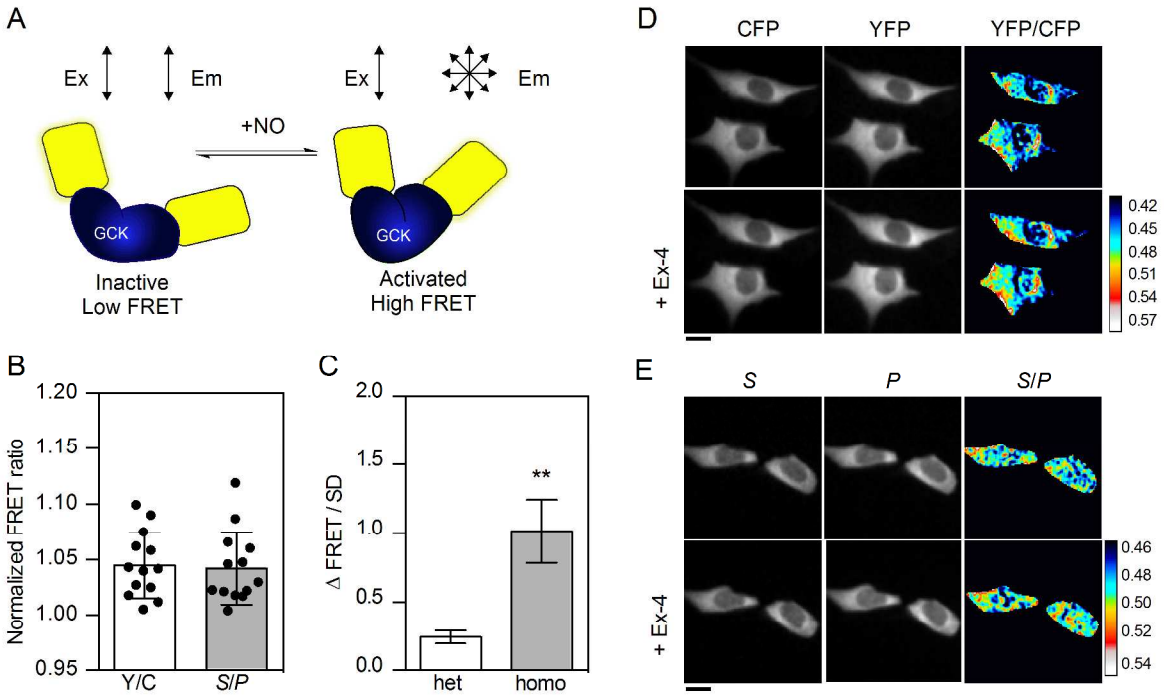

Figure 1. **Characterization of the homotransfer FRET–GCK biosensor.** (A) Schematic of the homotransfer FRET–GCK sensor. In the absence of FRET, illumination with polarized light produces emitted photons with a parallel polarization. FRET is depolarizing and results in the emission of randomly oriented photons relative to the illumination plane. (B) βTC3 cells transfected with the heterotransfer FRET–GCK sensor (*white*) or homotransfer FRET–GCK sensor (*gray*) were incubated in low glucose conditions for 3 h before imaging. Cells were pre-treated with 50 μM βME for 5 min before stimulation with 50 nM exendin-4 (Ex-4). FRET ratios were calculated 3 min post-stimulation with Ex-4 and normalized to pre-stimulation values. Error bars indicate SD. (C) The Δ FRET/ standard deviation value was calculated for the heterotransfer FRET–GCK sensor (*white*) or homotransfer FRET–GCK sensor (*gray*). Error bars indicate SEM. n = 13 cells, ** $p < 0.01$. (D) FRET map of the heterotransfer FRET–GCK sensor: CFP channel, YFP channel and the YFP/CFP ratio. (E) FRET map of homotransfer FRET–GCK sensor: *S* channel, *P* channel and the *S*/*P* ratio. The top rows of (D) and (E) show baseline fluorescence, and the bottom rows are after stimulation with 50 nM Ex-4 for 3 min. Areas of red indicate increased FRET and sensor activation. Scale bar = 10 μm.

used to quantify heterotransfer FRET. For homotransfer FRET, we illuminated the sample with polarized light and collected fluorescence emissions in geometries parallel (*P*) and perpendicular (*S*) to the illumination plane (Fig. 1A). Depolarized fluorescence from increased FRET (*32*) raises the calculated *S*/*P* ratio. Exendin-4 induced similar FRET ratio changes for each sensor (Fig. 1B). However, polarization measurements typically have a better signal-to-noise ratio compared to intensity-based measurements. Factoring in the standard deviation of baseline FRET ratios (*26*), conversion to the homotransfer strategy improved the dynamic range approximately 4-fold (Fig. 1C). Intensity maps of the FRET ratios depict areas of increased activation for the heterotransfer sensor and homotransfer sensor, respectively (Fig. 1D, 1E). Exendin-4 stimulation induced similar activation patterns across the two sensors.

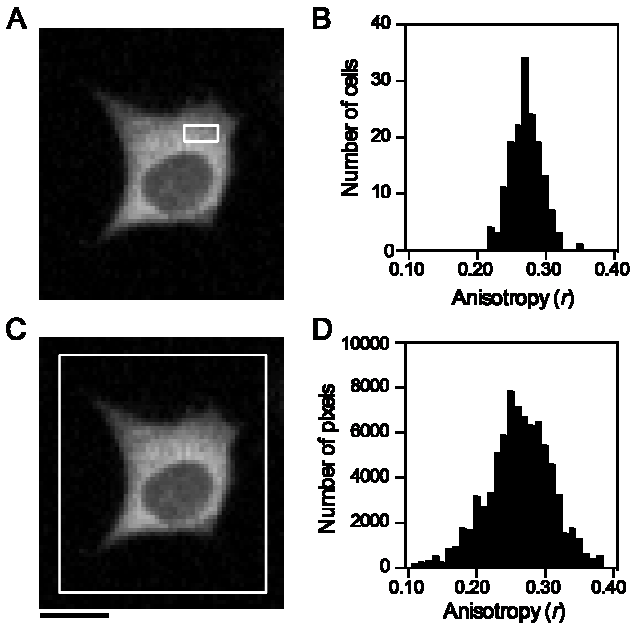

Figure 2. Automated pixel image processing for quantitative FRET measurements. βTC3 Cells transfected with the homotransfer FRET–GCK sensor were cultured in low glucose for 3 h and pre-treated with 50 μM βME for 5 min before imaging. Quantitative FRET measurements were made from (A) hand-selected regions of interest consisting of ~100 pixels from ~160 cells. The histogram of the anisotropy values is shown in (B), mean = 0.26, SD = 0.05; n ~160 regions of interest. (C) Anisotropy values were also calculated from individual pixels of each image of the same ~160 cells in (A,B) Scale bar = 10 μm (D) Histograms of the anisotropy values show the collective data, mean = 0.27, SD = 0.02; n ~80,000 pixels.

Automated pixel analysis

To facilitate quantitative analysis of the homotransfer FRET–GCK data, we normalized polarization values by calculating fluorescence anisotropies. Decreased anisotropy indicates increased depolarization from FRET. Our approach was also modified to enhance the statistical power of the data set. Previously, hand-drawn regions of interest of ~100 pixels were used to pool information together for FRET calculations (Fig. 2A, 2B). While data reduction in this manner is useful for quantifying cellular GCK dynamics, it also reduces the number of measurements and obscures the variability of the raw data. For more in-depth quantitative analyses, we calculated anisotropy values for each pixel (Fig. 2C, 2D). Saturated pixels and those with insufficient brightness above background were excluded from the analysis. Consideration of

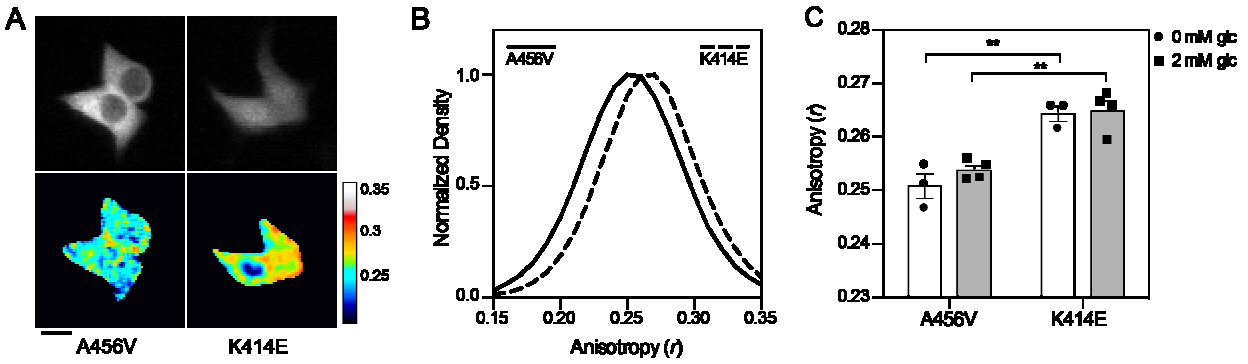

Figure 3. Active and Less-active GCK states. (A) Changes in the anisotropy of GCK(A456V) and GCK(K414E) are shown globally as an anisotropy map. Areas of blue indicate increased FRET. Scale bar = 10 µm. (B) A normalized density plot shows the distribution of anisotropy values for GCK(A456V) (*solid line*) and GCK(K414E) (*dashed line*); n ~500 cells; SD = 0.04. (C) Mean anisotropy values are plotted for each mutant incubated in glucose-free (*white*) or 2 mM glucose (*gray*) conditions for 3 h before experimentation; n = 3 or 4, each is an average of ~150 cells from a separate culture dish. Error bars = SEM. ** $p < 0.01$.

the anisotropy data at the pixel level increased the number of measurements from 160 cells to over 80,000 pixels.

FRET states resulting from GCK mutations

Point mutations were introduced into the GCK sensor to promote enzymatic states with high (A456V) and low (K414E) activity. The A456V mutation activates GCK independently of glucose and is associated with decreased blood glucose levels and hyperinsulinemia (*33*, *34*). Contrastingly, the K414E mutant is a known MODY2 mutation and shifts the activation curve to the right (*34*, *35*). An anisotropy map shows a higher amount of FRET with the GCK(A456V) mutant compared to the GCK(K414E) mutant (Fig. 3A). Areas of higher FRET–GCK activation are shown in blue. The density plot distribution (Fig. 3B) of pixel anisotropies under low glucose conditions also shows distinct differences. The inactive mutant is shifted towards higher anisotropies compared to GCK(A456V). Even so, the standard deviation of calculated anisotropies is approximately the same, suggesting that each mutant occupies a similar number of conformational states. We then pooled together data from several dishes (Fig. 3C). The mean anisotropies were ~ 0.25 for FRET–GCK(A456V) and ~ 0.26 for FRET–GCK(K414E). This difference was significant in both low glucose and glucose-free conditions (Fig. 3C). Glucose did not affect the anisotropy values for either mutant sensor (Fig. 3C), indicating their conformational states are glucose-independent.

Effects of a GCK activator on biosensor FRET

GCK activators (GKA) bind to a small pocket near the C-terminus of GCK that is lined by Ala456. To test whether these small molecules produce similar changes in FRET–GCK anisotropies as our activating mutant, βTC3 cells were treated with PF-04937319 (*36*) (Fig. 4). Activation of the sensor was observed throughout the cytoplasm (Fig. 4A). The FRET–GCK sensor reported an anisotropy of ~0.25 in the presence of the GKA (Fig. 4B, 4C) and was significantly reduced compared to untreated control cells (Fig. 4C). Further, the mean anisotropy value is shared by the activating A456V mutation, suggesting that the GKA and A456V induce similar conformational changes in GCK.

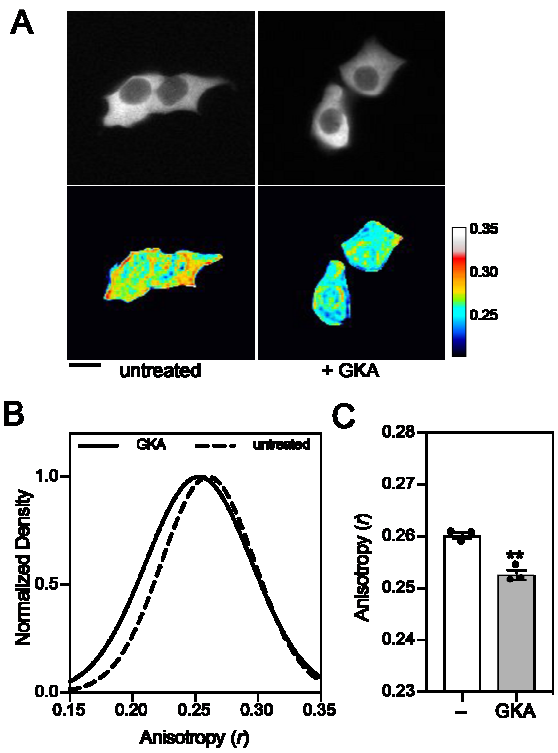

Figure 4. FRET–GCK response to a GCK activator. βTC3 cells expressing the homotransfer FRET–GCK sensor were cultured in imaging buffer with 2 mM glucose and 50 μM βME for 3 h. Cells were then either left untreated or stimulated with GKA (10 μM PF-04937319) immediately before image collection. Panel A shows representative anisotropy maps for the two conditions. Areas of blue indicate increased FRET. Scale bar = 10 μm. (B) Normalized density plots show FRET–GCK pixel anisotropies for GKA-treated (*solid line*) and control conditions (untreated, *dashed line*); n ~ 300 cells; SD = 0.04. The average anisotropies of cells left untreated (–, *white*) or treated with the GKA (*gray*) are shown in (C). n = 3 replicates, each n represents the mean *r* from ~100 cells from the same culture dish. Error bars = SEM. ** p <0.01.

Glucose-dependence of FRET–GCK activation

Next, we conducted a dose-response with glucose (Fig. 5A). Activation of the sensor displayed a sigmoidal relationship with glucose consistent with the enzymatic activity of endogenous GCK (*37*, *38*). Because 2 mM glucose is sub-threshold for GCK activation (*39*, *40*), we considered this to be indicative of the low activity, likely 'open', state. 25 mM glucose, while higher than β-cells ever experience *in vivo*, is commonly used to induce maximal GCK enzymatic activity in living cells (*41*, *42*). As expected, the change in FRET is significantly higher for the 25 mM glucose treated cells than for cells in 2 mM glucose. Representative images of the anisotropy values show increased activation in cells treated with 25 mM glucose (Fig. 5B). In 2 mM glucose conditions, the peak value for pixel anisotropies is ~0.26 and shifts to ~0.25 at 25 mM glucose (Fig. 5C).

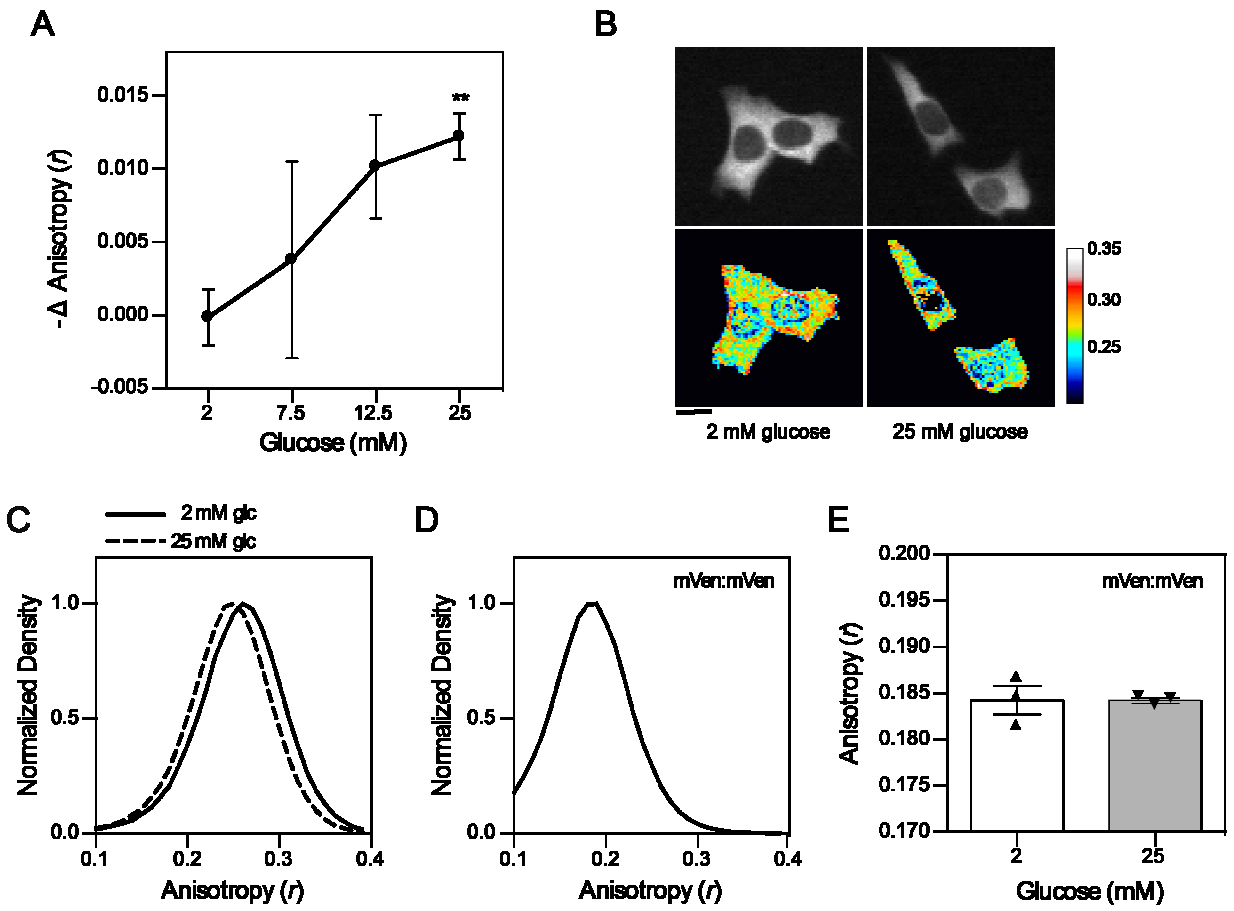

Figure 5. Glucose-dependence of the homotransfer FRET–GCK biosensor. (A) βTC3 cells with the homotransfer FRET–GCK sensor were incubated in low glucose media for 3 h before imaging. Cells were pre-treated with 50 μM βME for 5 min before stimulation. Pre-stimulation imaging media contained 2 mM glucose and was adjusted to final glucose concentrations of 2, 7.5, 12.5 or 25 mM as indicated. Images were collected of ~500 cells for each group. The mean –Δ anisotropy is plotted for clarity. Error bars = SEM; ** $p < 0.01$. (B) An anisotropy map shows the change between the 2 and 25 mM glucose conditions. Areas of blue indicate increased FRET. Scale bar = 10 μm. (C) The normalized density plot shows the anisotropy distribution of 2 mM glucose (*solid line*) and 25 mM glucose (*dashed line*); n ~500 cells; SD = 0.04. (D) The distribution of anisotropy values is shown from cells transfected with the mVenus tandem construct incubated in 2 mM glucose; n ~250 cells; SD = 0.04. The average anisotropies comparing 2 mM glucose (*white*) to 25 mM glucose (*gray*) are shown in (E) for the mVenus-mVenus construct; n = 3, each n is an average of ~150 cells. Error bars = SEM; $p > 0.05$.

To test for the potential effects of glucose on FRET independently of GCK, we removed GCK from the biosensor to create a tandem mVenus–mVenus dimer separated by a short linker sequence. The density plot distribution of the mVenus-mVenus construct (Fig. 5D) reveals a much lower anisotropy (indicating increased FRET) than the GCK homotransfer sensor at 2 mM glucose (Fig. 5C). The average anisotropies of the tandem fusion were not affected by low or high glucose conditions (Fig. 5E). These results indicate that glucose alone does not change FP anisotropy in the absence of the GCK protein sequence.

To explore the effect of glucose-free conditions on GCK conformation in living cells (*10*), βTC3 cells transfected with the GCK homotransfer sensor were cultured in 2 mM glucose

or glucose-free media for 3 h before imaging (Fig. 6A, 6B). The average FRET–GCK pixel anisotropies (Fig. 6A) and density plot distributions (Fig. 6B) were not significantly different between these conditions, suggesting a single detectable state in low glucose and glucose-free conditions.

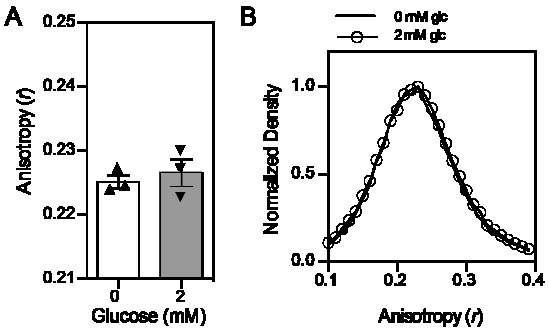

Figure 6. Glucose-independent mVenus fluorescence. (A) Mean anisotropy values for the homotransfer FRET–GCK sensor in cells cultured in glucose-free (*white*) or low glucose (*gray*) conditions for 3 h before imaging; n = 3, each n is an average of ~50 cells. Error bars = SEM. (B) Distribution of anisotropy values of the same cells in (A) incubated in glucose-free (*solid line*) or low glucose (*open circles*) conditions; n ~150; SD = 0.04.

NO facilitates the transition of GCK to the activated state

Previously, we reported that S-nitrosylation participates in GCK activation by hormone-activated receptors (*25*). To further understand how NO regulates GCK, βTC3 cells were transfected with the homotransfer FRET–GCK sensor and incubated in low-glucose conditions as before. Cells were then treated with either S-Nitroso-N-acetyl-DL-penicillamine (SNAP) to stimulate GCK S-nitrosylation, or β-Mercaptoethanol (βME), a disulfide bond reducing agent, for 5 min before imaging. The anisotropy map (Fig. 7A) depicts the range of values measured from a representative cell from each treatment with areas of increased GCK activation in blue.

SNAP-treated cells have increased GCK sensor activation compared to βME treated cells (Fig. 7B). The average FRET value for the cells treated with SNAP is ~0.25 while the average FRET value for the βME treated cells is ~0.26 (Fig. 7C). Even so, SNAP can promote protein S-nitrosylation through varied mechanisms beyond chemical release of NO (*43*, *44*). Stimulation of cells with a strict chemical NO releasing agent, 2-(N, N- diethylami no)-diazenolate-2-oxide (DEANO) (*45*, *46*), also stimulated FRET-GCK biosensor activation compared to cells treated with βME (Fig. 7D). To further examine the mechanism underlying SNAP-mediated GCK activation, we utilized a FRET–GCK sensor that lacks the S-nitrosylation site. The C371S mutation has been previously shown to block GCK S-nitrosylation (*15*). Stimulation with SNAP (Fig. 7E) or high glucose (Fig. 7F) did not significantly change the fluorescence anisotropy of the C371S mutant FRET–GCK sensor in βTC3 cells. Notably, the anisotropy values observed in the presence of SNAP, DEANO and βME converged with the measurements made using the high and low GCK activity mutants (Fig. 3C), and high and low glucose concentrations (Fig.

5C). These data suggest that S-nitrosylation facilitates GCK transition to the same activated conformational state that is also induced by 25 mM glucose, GKAs, or GCK(A456V).

Discussion

Overall, FRET–GCK biosensors, and generally GCK-FP fusions, have proved to be useful probes for understanding GCK regulation in living cells. FP fusion to either the N- or C- termini does not affect GCK localization (*13*, *23*), and expression of WT GCK-YFP fusion proteins does not alter β-cell metabolism in culture (*24*). GCK-FP fusions are S-nitrosylated (*15*), can bind to known GCK-binding proteins (*25*, *47*, *48*), and are also cleared through the ubiquitin-proteasome mediated pathway like the native GCK protein (*49*). Finally, Ca^{2+} dependent GCK activation of FRET–GCK sensors through the NO pathway precisely agrees with the Ca^{2+}

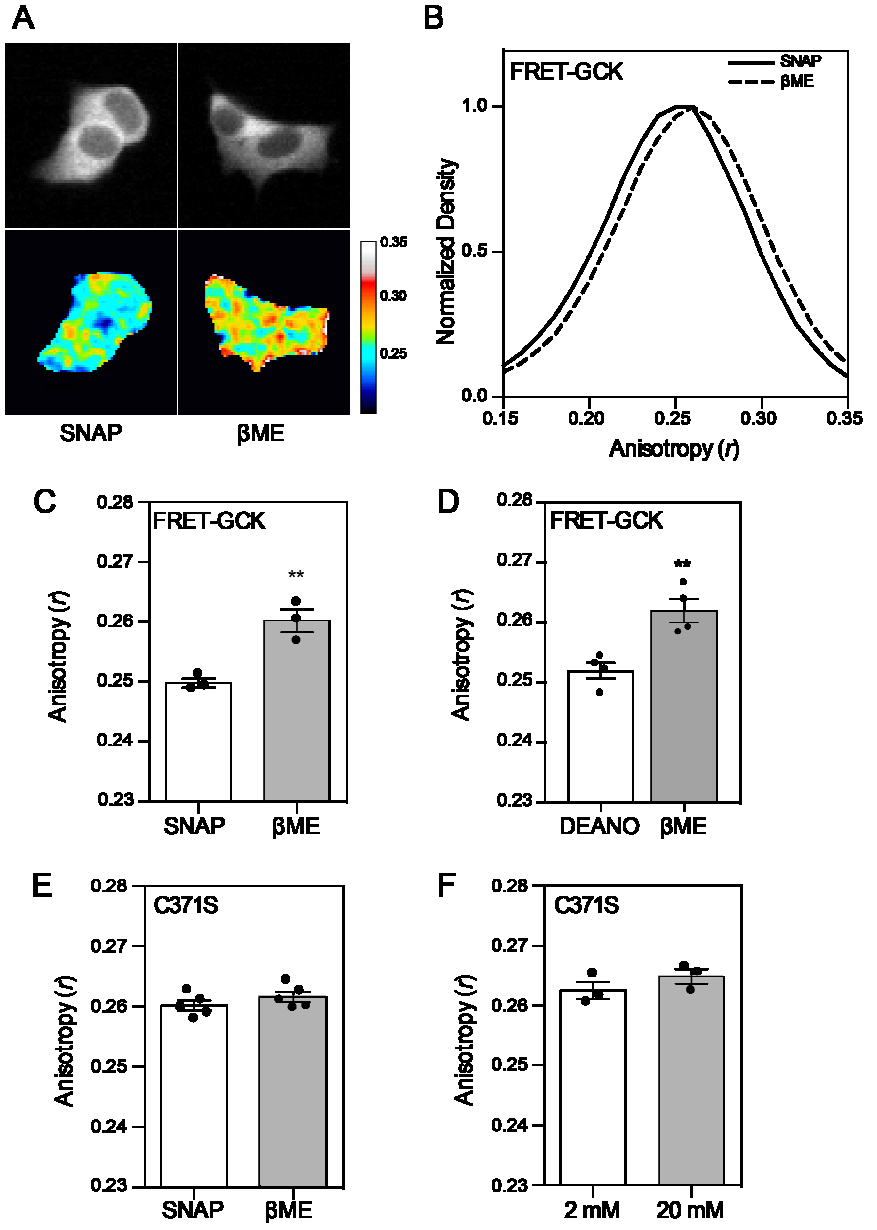

Figure 7. NO facilitates the transition of GCK to the active state. Cells with the homotransfer FRET–GCK sensor were cultured in low glucose for 3 h before imaging. (A) Anisotropy map of cells treated with 100 μM SNAP or 50 μM βME for 5 min before image collection. Areas of blue indicate increased FRET. Scale bar = 10 μm. (B) The normalized distribution plots of SNAP (*solid line*) and βME (*dashed line*); n ~450 cells; SD = 0.04. The average anisotropies of SNAP (*white*) and βME (*gray*) are shown in (C). n = 3, each n is an average of ~150 cells. Error bars = SEM. ** $p < 0.01$. (D). Cells plated as in (C) were treated with either 100 μM DEANO or βME. n=4; error bars = SEM; ** $p < 0.01$. (E, F) Cells expressing a FRET–GCK sensor with a mutated S-nitrosylation site (C371S) were treated with SNAP (E), βME (E), or the indicated glucose concentrations (F). Each n is the average of ~75 cells. Results were not significant by t-test ($p > 0.05$).

concentration required to activate neuronal nitric oxide synthase (nNOS) (*25*). Together, these previous studies show that fusion of FPs to GCK is minimally perturbing to GCK structure and cellular regulation.

Use of FPs to measure changes in protein conformation requires additional consideration because the large FP size limits their rotational mobility and makes calculations of distance more difficult. Further, FPs tend to be less bright and have greater spectral overlap than the organic fluorophores typically used for structure determination. Standard data reduction strategies including pixel binning, image smoothing, and using calculations of normalized regions of interest are used to improve the signal-to-noise of the FRET measurements.

Compared to intensity-based approaches, polarization eliminates the need to correct for fluorescence crosstalk and delivers 10-fold more precise measurements (*18*, *50–53*). The improved data quality enables analysis of pixel anisotropies. This enhances our statistical power by increasing the number of measures ~500-fold. The enhanced Δ FRET/standard deviation value means that we can better distinguish between small changes in FRET. While there is overlap, the average anisotropy value of each state is significantly different. The high precision and contrast of the homotransfer anisotropy sensor coupled with the individual pixel analysis, allows us to quantify small anisotropy differences reliably. Thus, we can perform an extensive quantitative analysis of FRET–GCK image data that permits extraction of two likely GCK FRET states.

The effects of MODY mutations on GCK conformation.

We chose GCK mutations A456V and K414E because of their likely influence on GCK conformational states. Ala456 is located in the allosteric binding pocket formed by the C-terminus and the small domain (*54*). This allosteric binding site is shared by all of the recently developed GKAs, and thus it is not surprising that GCK(A456V) similarly enhances glucose affinity and catalytic efficiency (*34*, *36*). Conversely, Lys414 is located in an alpha helix that participates in ATP binding (*54*). While the K414E mutation does reduce ATP affinity, it also reduces affinity for glucose to a comparable degree (*54*), suggesting that the reduced activity of this mutant reflects a conformational shift in GCK.

Two measurable GCK conformations in living cells

FRET efficiency is steeply dependent on the distance separating the donor and acceptor. Even a 1 nm increase between the FRET pair can reduce FRET efficiency by as much as 50% (*32*). This steep distance-dependence has made FRET quite useful for mapping protein structures and tracking the conformational dynamics of small globular proteins (*55–59*), similar to GCK. Thus, FRET provides sufficient spatial sensitivity to track complex protein conformational changes and multiple states of interaction.

The anisotropy distribution for the activated FRET–GCK(A456V) mutant is shared by the activated WT FRET–GCK sensor stimulated by either high glucose, NO or a GKA. Similarly, the distribution of the inactivated FRET–GCK(K414E) sensor is shared by the WT FRET–GCK sensor in the absence of glucose, under low glucose conditions, and in cells treated with βME. Furthermore, the SD for each condition is 0.04, and is equivalent to the SD for the mVenus tandem dimer. Together, these observations support that each condition represents one of two measureable GCK conformations in living cells. This is supported by studies monitoring the intrinsic fluorescence of GCK with stopped-flow fluorimetry (*8*), which also reported only two identifiable states in recombinent GCK preparations. Importantly, our study relies on steady-state fluorescence measurements that are unlikely to pick up intermediate conformational transitions.

Interestingly, we do not see any difference in FRET between low and glucose-free conditions. Our observation is counter to structural studies that have identified an inactive 'super-open' glucose-free conformation that contains a partially unfolded small domain (*10*). If the large change in GCK conformation between the 'super-open' and 'open' conformations is also 12°, as it is for hexokinase I (*10*), FRET measurements would almost certainly be able to distinguish between the two proposed glucose-free states given the magnitude of the conformational change.

Even so, the distribution of anisotropy values for the FRET–GCK sensor does not skew or shift when cells are incubated in glucose-free conditions rather than 2 mM glucose (Fig. 6). Cytoplasmic glucose levels roughly equilibrate with the extracellular glucose due to the presence of GLUT2 glucose transporters in islets (*60*, *61*) and β-cells (*62*). Exposure to low glucose levels (< 1 mM) has been shown to deplete intracellular glucose concentrations to a fraction of the extracellular concentration within 3 h (*62*). After 3 h incubation in glucose-free or 2 mM glucose media, we do not report a bimodal distribution in either condition. These data suggest a singular GCK conformation exists in living β-cells under low glucose conditions.

It is also noteworthy that the low glucose experiments utilize concentrations below the physiologic range. Fasting blood glucose levels are generally around 3.5 – 5.5 mM in healthy individuals whereas clinical hypoglycemia occurs in the 2-3 mM range (*63*). Fasting blood sugar remains above 2 mM even in patients with genetically-linked persistent hyperinsulinemic hypoglycemia of infancy (*1*). Thus, it is unclear whether physiological conditions would permit formation of the proposed apo-glucose GCK conformations *in vivo*.

GCK regulation by S-nitrosylation

Our evidence suggests that elevated glucose and S-nitrosylation both induce the same high-activity GCK conformational state. The distribution of FRET–GCK anisotropy values was the same for 25 mM glucose (Fig. 5C) and SNAP-induced (Fig. 7B) conformational states. Additionally, the distribution was also shared with a FRET–GCK sensor containing the A456V activating mutation (Fig. 3B). All three treatments are associated with enhanced GCK activity (*25*, *33*, *64*) suggesting a shared conformational state that is highly active. Conversely, deactivating conditions, 2 mM glucose (Fig. 5C), denitrosylation with βME (Fig. 7B) and the K414E inactivating mutation (Fig. 3B), also converged on a single FRET–GCK anisotropy distribution.

Physiologic regulation of GCK

Our findings also point to the importance of NO in activating GCK. The glucose levels (~25 mM) needed to activate GCK efficiently are outside the physiologic range of 4-8 mM (*65*). 7.5 mM glucose is not only within the postprandial blood glucose range but is also the glucose concentration at which half-maximal activation of GCK occurs (*3*). At this concentration, FRET ratios are highly variable, suggesting a mixture of activated and inactivated conformations (Fig. 5A). If an intermediate conformation existed, we would expect the variability to be much smaller, similar to those of the 2 mM or 25 mM groups. Our data suggest that S-nitrosylation facilitates GCK's transition to the higher activity state and stabilizes the fully active conformation.

References

1. Gloyn, A. L.; Odili, S.; Buettger, C.; Njolstad, P. R.; Shiota, C.; Magnuson, M. A.; Matschinsky, F. M. (2004) Glucokinase and the Regulation of Blood Sugar, in *Glucokinase and Glycemic Disease: From Basics to Novel Therapeutics* (Matschinsky, F. M.; Magnuson, M. A., Eds.) pp 92-109, KARGER, Basel.
2. Glaser, B.; Kesavan, P.; Heyman, M.; Davis, E.; Cuesta, A.; Buchs, A.; Stanley, C. A.; Thornton, P. S.; Permutt, M. A.; Matschinsky, F. M.; Herold, K. C. (1998) Familial hyperinsulinism caused by an activating glucokinase mutation. *N. Engl. J. Med. 338*, 226-230.
3. Gloyn, A. L. (2003) Glucokinase (GCK) mutations in hyper- and hypoglycemia: maturity-onset diabetes of the young, permanent neonatal diabetes, and hyperinsulinemia of infancy. *Human Mutation 22*, 353-362.
4. Bontemps, F.; Hue, L.; Hers, H. G. (1978) Phosphorylation of glucose in isolated rat hepatocytes. Sigmoidal kinetics explained by the activity of glucokinase alone. *Biochem. J. 174*, 603-611.
5. Cornish-Bowden, A.; Storer, A. C. (1986) Mechanistic origin of the sigmoidal rate behaviour of rat liver hexokinase D ('glucokinase'). *Biochem. J. 240*, 293-296.
6. Fridlyand, L. E.; Phillipson, L. H. (2011) Mechanisms of glucose sensing in the pancreatic beta-cell: A computational systems-based analysis. *Islets 3*, 224-230.
7. Byrne, M. M.; Sturis, J.; Clément, K.; Vionnet, N.; Pueyo, M. E.; Stoffel, M.; Takeda, J.; Passa, P.; Cohen, D.; Bell, G. I. (1994) Insulin secretory abnormalities in subjects with hyperglycemia due to glucokinase mutations. *J. Clin. Invest. 93*, 1120-1130.
8. Heredia, V. V.; Thomson, J.; Nettleton, D.; Sun, S. (2006) Glucose-induced conformational changes in glucokinase mediate allosteric regulation: transient kinetic analysis. *Biochemistry 45*, 7553-7562.
9. Larion, M.; Hansen, A. L.; Zhang, F.; Bruschweiler-Li, L.; Tugarinov, V.; Miller, B. G.; Brüschweiler, R. (2015) Kinetic Cooperativity in Human Pancreatic Glucokinase Originates from Millisecond Dynamics of the Small Domain. *Angew Chem Int Ed Engl 54*, 8129-8132.
10. Kamata, K.; Mitsuya, M.; Nishimura, T.; Eiki, J.; Nagata, Y. (2004) Structural basis for allosteric regulation of the monomeric allosteric enzyme human glucokinase. *Structure 12*, 429-438.
11. Zhang, J.; Li, C.; Shi, T.; Chen, K.; Shen, X.; Jiang, H. (2009) Lys169 of human glucokinase is a determinant for glucose phosphorylation: implication for the atomic mechanism of glucokinase catalysis. *PLoS One 4*, e6304.
12. Larion, M.; Salinas, R. K.; Bruschweiler-Li, L.; Miller, B. G.; Bruschweiler, R. (2012) Order-disorder transitions govern kinetic cooperativity and allostery of monomeric human glucokinase. *PLoS Biol. 10*, e1001452.
13. Baltrusch, S.; Lenzen, S. (2007) Novel insights into the regulation of the bound and diffusible glucokinase in MIN6 beta-cells. *Diabetes 56*, 1305-1315.
14. Massa, L.; Baltrusch, S.; Okar, D. A.; Lange, A. J.; Lenzen, S.; Tiedge, M. (2004) Interaction of 6-phosphofructo-2-kinase/fructose-2,6-bisphosphatase (PFK-2/FBPase-2) with glucokinase activates glucose phosphorylation and glucose metabolism in insulin-producing cells. *Diabetes 53*, 1020-1029.
15. Rizzo, M. A.; Piston, D. W. (2003) Regulation of beta cell glucokinase by S-nitrosylation and association with nitric oxide synthase. *J. Cell Biol. 161*, 243-248.

16. Efrat, S.; Fejer, G.; Brownlee, M.; Horwitz, M. S. (1995) Prolonged survival of pancreatic islet allografts mediated by adenovirus immunoregulatory transgenes. *Proc. Natl. Acad. Sci. U S A 92*, 6947-6951.
17. Ding, S. Y.; Nkobena, A.; Kraft, C. A.; Markwardt, M. L.; Rizzo, M. A. (2011) Glucagon-like peptide 1 stimulates post-translational activation of glucokinase in pancreatic beta cells. *J. Biol. Chem. 286*, 16768-16774.
18. Piston, D. W.; Rizzo, M. A. (2008) FRET by fluorescence polarization microscopy. *Methods Cell Biol. 85*, 415-430.
19. Markwardt, M. L.; Snell, N. E.; Guo, M.; Wu, Y.; Christensen, R.; Liu, H.; Shroff, H.; Rizzo, M. A. (2018) A Genetically Encoded Biosensor Strategy for Quantifying Non-muscle Myosin II Phosphorylation Dynamics in Living Cells and Organisms. *Cell Reports 24*, 1060-1070.e4.
20. Ross, B. L.; Tenner, B.; Markwardt, M. L.; Zviman, A.; Shi, G.; Kerr, J. P.; Snell, N. E.; McFarland, J. J.; Mauban, J. R.; Ward, C. W.; Rizzo, M. A.; Zhang, J. (2018) Single-color, ratiometric biosensors for detecting signaling activities in live cells. *Elife 7*, e35458.
21. Schindelin, J.; Arganda-Carreras, I.; Frise, E.; Kaynig, V.; Longair, M.; Pietzsch, T.; Preibisch, S.; Rueden, C.; Saalfeld, S.; Schmid, B.; Tinevez, J. Y.; White, D. J.; Hartenstein, V.; Eliceiri, K.; Tomancak, P.; Cardona, A. (2012) Fiji: an open-source platform for biological-image analysis. *Nat Methods 9*, 676-682.
22. Pau, G.; Fuchs, F.; Sklyar, O.; Boutros, M.; Huber, W. (2010) EBImage--an R package for image processing with applications to cellular phenotypes. *Bioinformatics 26*, 979-981.
23. Rizzo, M. A.; Magnuson, M. A.; Drain, P. F.; Piston, D. W. (2002) A functional link between glucokinase binding to insulin granules and conformational alterations in response to glucose and insulin. *J. Biol. Chem. 277*, 34168-34175.
24. Ding, S. Y.; Tribble, N. D.; Kraft, C. A.; Markwardt, M.; Gloyn, A. L.; Rizzo, M. A. (2010) Naturally occurring glucokinase mutations are associated with defects in posttranslational S-nitrosylation. *Mol. Endocrinol. 24*, 171-177.
25. Markwardt, M. L.; Nkobena, A.; Ding, S. Y.; Rizzo, M. A. (2012) Association with nitric oxide synthase on insulin secretory granules regulates glucokinase protein levels. *Mol. Endocrinol. 26*, 1617-1629.
26. Markwardt, M. L.; Seckinger, K. M.; Rizzo, M. A. (2016) Regulation of Glucokinase by Intracellular Calcium Levels in Pancreatic beta Cells. J. Biol. Chem. 291, 3000-3009.
27. Woehler, A.; Wlodarczyk, J.; Neher, E. (2010) Signal/noise analysis of FRET-based sensors. *Biophys. J. 99*, 2344-2354.
28. Rizzo, M. A.; Springer, G.; Segawa, K.; Zipfel, W. R.; Piston, D. W. (2006) Optimization of pairings and detection conditions for measurement of FRET between cyan and yellow fluorescent proteins. *Microsc Microanal 12*, 238-254.
29. Zimmermann, T.; Rietdorf, J.; Girod, A.; Georget, V.; Pepperkok, R. (2002) Spectral imaging and linear un-mixing enables improved FRET efficiency with a novel GFP2-YFP FRET pair. *FEBS Lett. 531*, 245-249.
30. Dhanesha, N.; Joharapurkar, A.; Shah, G.; Dhote, V.; Kshirsagar, S.; Bahekar, R.; Jain, M. (2012) Exendin-4 ameliorates diabetic symptoms through activation of glucokinase. *J Diabetes 4*, 369-377.
31. Park, J. H.; Kim, S. J.; Park, S. H.; Son, D. G.; Bae, J. H.; Kim, H. K.; Han, J.; Song, D. K. (2012) Glucagon-like peptide-1 enhances glucokinase activity in pancreatic beta-cells through the association of Epac2 with Rim2 and Rab3A. *Endocrinology 153*, 574-582.
32. Förster, T. (1948) Zwischenmolekulare energiewanderung und fluo- reszenz., english translation. *Ann. Phys. 6*, 54-75.

33. Christesen, H. B.; Jacobsen, B. B.; Odili, S.; Buettger, C.; Cuesta-Munoz, A.; Hansen, T.; Brusgaard, K.; Massa, O.; Magnuson, M. A.; Shiota, C.; Matschinsky, F. M.; Barbetti, F. (2002) The second activating glucokinase mutation (A456V): implications for glucose homeostasis and diabetes therapy. *Diabetes 51*, 1240-1246.
34. Pino, M. F.; Kim, K. A.; Shelton, K. D.; Lindner, J.; Odili, S.; Li, C.; Collins, H. W.; Shiota, M.; Matschinsky, F. M.; Magnuson, M. A. (2007) Glucokinase thermolability and hepatic regulatory protein binding are essential factors for predicting the blood glucose phenotype of missense mutations. *J. Biol. Chem. 282*, 13906-13916.
35. Davis, E. A.; Cuesta-Munoz, A.; Raoul, M.; Buettger, C.; Sweet, I.; Moates, M.; Magnuson, M. A.; Matschinsky, F. M. (1999) Mutants of glucokinase cause hypoglycaemia- and hyperglycaemia syndromes and their analysis illuminates fundamental quantitative concepts of glucose homeostasis. *Diabetologia 42*, 1175-1186.
36. Pfefferkorn, J. A.; Guzman-Perez, A.; Oates, P. J.; Litchfield, J.; Aspnes, G.; Basak, A.; Benbow, J.; Berliner, M. A.; Bian, J.; Choi, C.; Freeman-Cook, K.; Corbett, J. W.; Didiuk, M.; Dunetz, J. R.; Filipski, K. J.; Hungerford, W. M.; Jones, C. S.; Karki, K.; Ling, A.; Li, J.-C.; Patel, L.; Perreault, C.; Risley, H.; Saenz, J.; Song, W.; Tu, M.; Aiello, R.; Atkinson, K.; Barucci, N.; Beebe, D.; Bourassa, P.; Bourbounais, F.; Brodeur, A. M.; Burbey, R.; Chen, J.; D'Aquila, T.; Derksen, D. R.; Haddish-Berhane, N.; Huang, C.; Landro, J.; Lee Lapworth, A.; MacDougall, M.; Perregaux, D.; Pettersen, J.; Robertson, A.; Tan, B.; Treadway, J. L.; Liu, S.; Qiu, X.; Knafels, J.; Ammirati, M.; Song, X.; DaSilva-Jardine, P.; Liras, S.; Sweet, L.; Rolph, T. P. (2011) Designing glucokinase activators with reduced hypoglycemia risk: discovery of N,N-dimethyl-5-(2-methyl-6-((5-methylpyrazin-2-yl)-carbamoyl)benzofuran-4-yloxy)pyrimidine-2-carboxamide as a clinical candidate for the treatment of type 2 diabetes mellitus. *MedChemComm 2*, 828.
37. Niemeyer, H.; de la Luz Cárdenas, M.; Rabajille, E.; Ureta, T.; Clark-Turri, L.; Peñaranda, J. (1975) Sigmoidal kinetics of glucokinase. *Enzyme 20*, 321-333.
38. Meglasson, M. D.; Burch, P. T.; Berner, D. K.; Najafi, H.; Vogin, A. P.; Matschinsky, F. M. (1983) Chromatographic resolution and kinetic characterization of glucokinase from islets of Langerhans. *Proc. Natl. Acad. Sci. U S A 80*, 85-89.
39. Weir, G. C.; Mojsov, S.; Hendrick, G. K.; Habener, J. F. (1989) Glucagonlike peptide I (7-37) actions on endocrine pancreas. *Diabetes 38*, 338-342.
40. Zelent, D.; Najafi, H.; Odili, S.; Buettger, C.; Weik-Collins, H.; Li, C.; Doliba, N.; Grimsby, J.; Matschinsky, F. M. (2005) Glucokinase and glucose homeostasis: proven concepts and new ideas. Biochem. *Soc.Trans. 33*, 306-310.
41. Liang, Y.; Najafi, H.; Matschinsky, F. M. (1990) Glucose regulates glucokinase activity in cultured islets from rat pancreas. *J. Biol. Chem. 265*, 16863-16866.
42. Matschinsky, F. M.; Magnuson, M. A.; Zelent, D.; Jetton, T. L.; Doliba, N.; Han, Y.; Taub, R.; Grimsby, J. (2006) The network of glucokinase-expressing cells in glucose homeostasis and the potential of glucokinase activators for diabetes therapy. *Diabetes 55*, 1-12.
43. Singh, R. J.; Hogg, N.; Joseph, J.; Kalyanaraman, B. (1996) Mechanism of Nitric Oxide Release fromS-Nitrosothiols. *J. Biol. Chem. 271*, 18596-18603.
44. Williams, D. L. H. (1999) The Chemistry of S-Nitrosothiols. *Accounts of Chemical Research 32*, 869-876.
45. Maragos, C. M.; Morley, D.; Wink, D. A.; Dunams, T. M.; Saavedra, J. E.; Hoffman, A.; Bove, A. A.; Isaac, L.; Hrabie, J. A.; Keefer, L. K. (1991) Complexes of.NO with nucleophiles as agents for the controlled biological release of nitric oxide. Vasorelaxant effects. *J. Med. Chem. 34*, 3242-3247.

46. Liang, H.; Nacharaju, P.; Friedman, A.; Friedman, J. M. (2015) Nitric oxide generating/releasing materials. *Future Sci OA 1*,
47. Baltrusch, S.; Francini, F.; Lenzen, S.; Tiedge, M. (2005) Interaction of glucokinase with the liver regulatory protein is conferred by leucine-asparagine motifs of the enzyme. *Diabetes 54*, 2829-2837.
48. Langer, S.; Kaminski, M. T.; Lenzen, S.; Baltrusch, S. (2010) Endogenous activation of glucokinase by 6-phosphofructo-2-kinase/fructose-2,6-bisphosphatase is glucose dependent. *Mol. Endocrinol. 24*, 1988-1997.
49. Hofmeister-Brix, A.; Lenzen, S.; Baltrusch, S. (2013) The ubiquitin-proteasome system regulates the stability and activity of the glucose sensor glucokinase in pancreatic β-cells. *Biochem. J. 456*, 173-184.
50. Axelrod, D. (1989) Fluorescence polarization microscopy. Methods Cell Biol. 30, 333-352.
51. Inoue, S.; Shimomura, O.; Goda, M.; Shribak, M.; Tran, P. T. (2002) Fluorescence polarization of green fluorescence protein. *Proc. Natl. Acad. Sci. U S A 99*, 4272-4277.
52. Mattheyses, A. L.; Kampmann, M.; Atkinson, C. E.; Simon, S. M. (2010) Fluorescence anisotropy reveals order and disorder of protein domains in the nuclear pore complex. *Biophys. J. 99*, 1706-1717.
53. Rizzo, M. A.; Piston, D. W. (2005) High-contrast imaging of fluorescent protein FRET by fluorescence polarization microscopy. *Biophys. J. 88*, L14-6.
54. Liu, S.; Ammirati, M. J.; Song, X.; Knafels, J. D.; Zhang, J.; Greasley, S. E.; Pfefferkorn, J. A.; Qiu, X. (2012) Insights into mechanism of glucokinase activation: observation of multiple distinct protein conformations. *J. Biol. Chem. 287*, 13598-13610.
55. Stryer, L.; Haugland, R. P. (1967) Energy transfer: a spectroscopic ruler. *Proc. Natl. Acad. Sci. U S A 58*, 719-726.
56. McWherter, C. A.; Haas, E.; Leed, A. R.; Scheraga, H. A. (1986) Conformational unfolding in the N-terminal region of ribonuclease A detected by nonradiative energy transfer. *Biochemistry 25*, 1951-1963.
57. Kenworthy, A. K. (2001) Imaging protein-protein interactions using fluorescence resonance energy transfer microscopy. *Methods 24*, 289-296.
58. Navon, A.; Ittah, V.; Landsman, P.; Scheraga, H. A.; Haas, E. (2001) Distributions of intramolecular distances in the reduced and denatured states of bovine pancreatic ribonuclease A. Folding initiation structures in the C-terminal portions of the reduced protein. *Biochemistry 40*, 105-118.
59. Raicu, V.; Stoneman, M. R.; Fung, R.; Melnichuk, M.; Jansma, D. B.; Pisterzi, L. F.; Rath, S.; Fox, M.; Wells, J. W.; Saldin, D. K. (2009) Determination of supramolecular structure and spatial distribution of protein complexes in living cells. Nature Photonics 3, 107.
60. Matschinsky, F. M.; Ellerman, J. E. (1968) Metabolism of glucose in the islets of Langerhans. *J. Biol. Chem. 243*, 2730-2736.
61. Tal, M.; Liang, Y.; Najafi, H.; Lodish, H. F.; Matschinsky, F. M. (1992) Expression and function of GLUT-1 and GLUT-2 glucose transporter isoforms in cells of cultured rat pancreatic islets. *J. Biol. Chem. 267*, 17241-17247.
62. Whitesell, R. R.; Powers, A. C.; Regen, D. M.; Abumrad, N. A. (1991) Transport and metabolism of glucose in an insulin-secreting cell line.beta.TC-1. *Biochemistry 30*, 11560-11566.
63. Alberti, K. G.; Zimmet, P. Z. (1998) Definition, diagnosis and classification of diabetes mellitus and its complications. Part 1: diagnosis and classification of diabetes mellitus provisional report of a WHO consultation. *Diabet Med 15*, 539-553.

64. Liang, Y.; Najafi, H.; Smith, R. M.; Zimmerman, E. C.; Magnuson, M. A.; Tal, M.; Matschinsky, F. M. (1992) Concordant glucose induction of glucokinase, glucose usage, and glucose-stimulated insulin release in pancreatic islets maintained in organ culture. *Diabetes 41*, 792-806.
65. Matschinsky, F.; Liang, Y.; Kesavan, P.; Wang, L.; Froguel, P.; Velho, G.; Cohen, D.; Permutt, M. A.; Tanizawa, Y.; Jetton, T. L.; et, A. (1993) Glucokinase as pancreatic beta cell glucose sensor and diabetes gene. *J. Clin. Invest. 92*, 2092-2098.

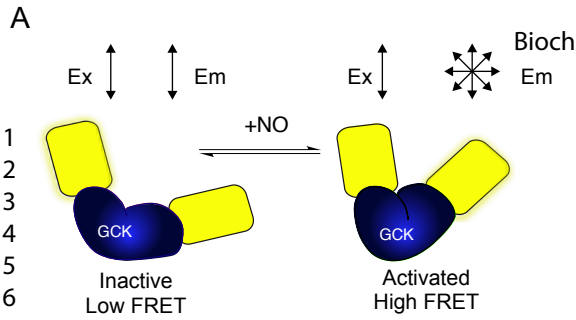

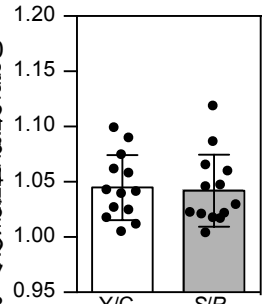

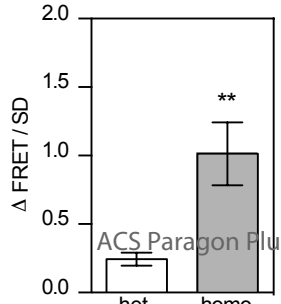

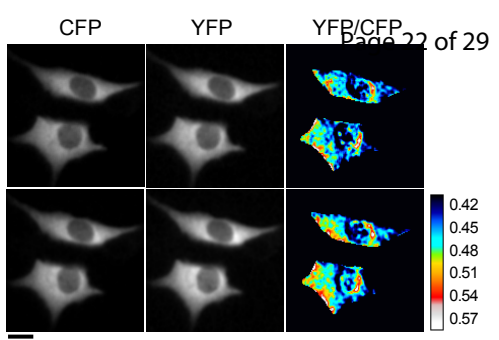

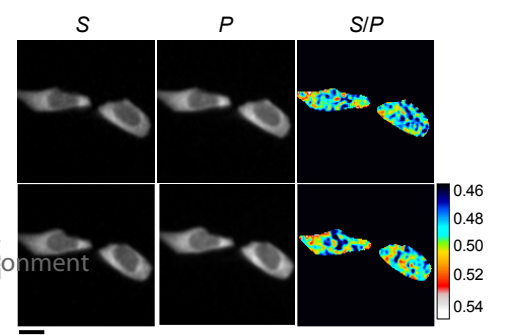

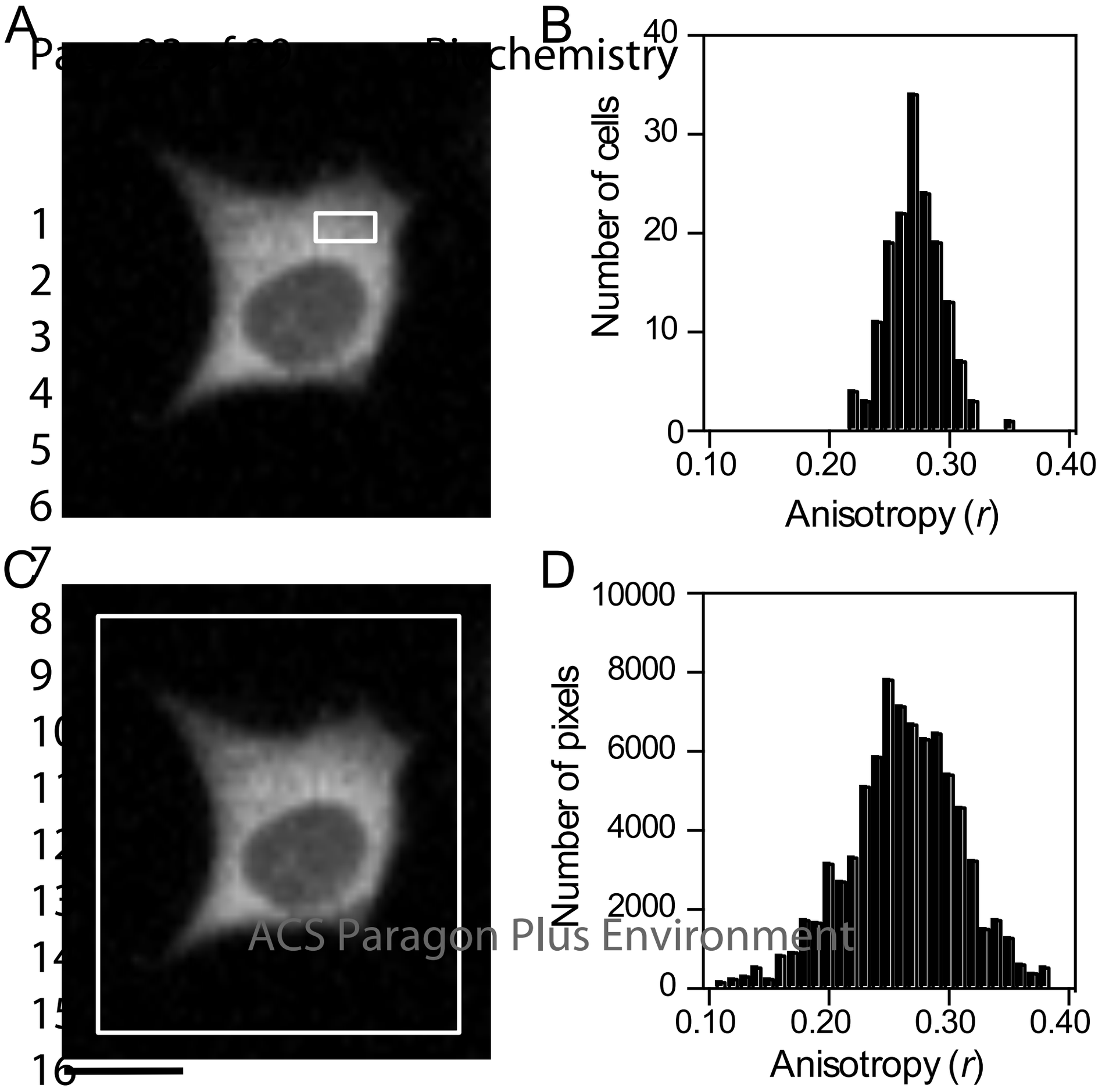

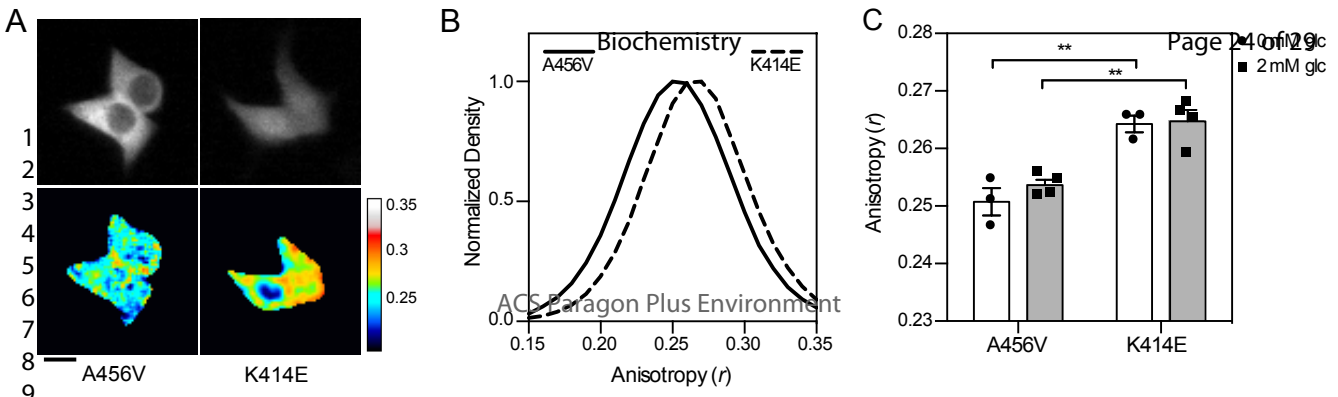

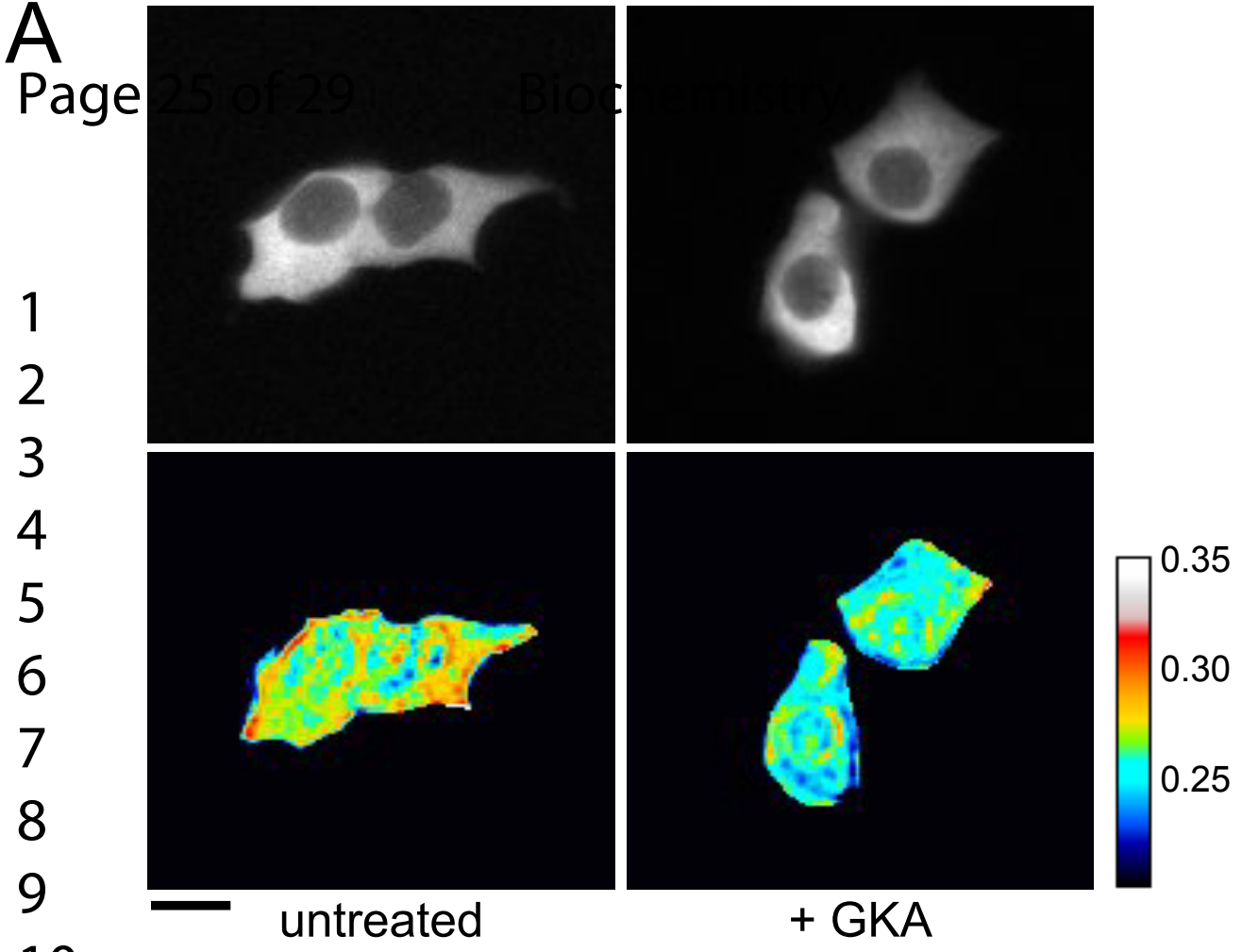

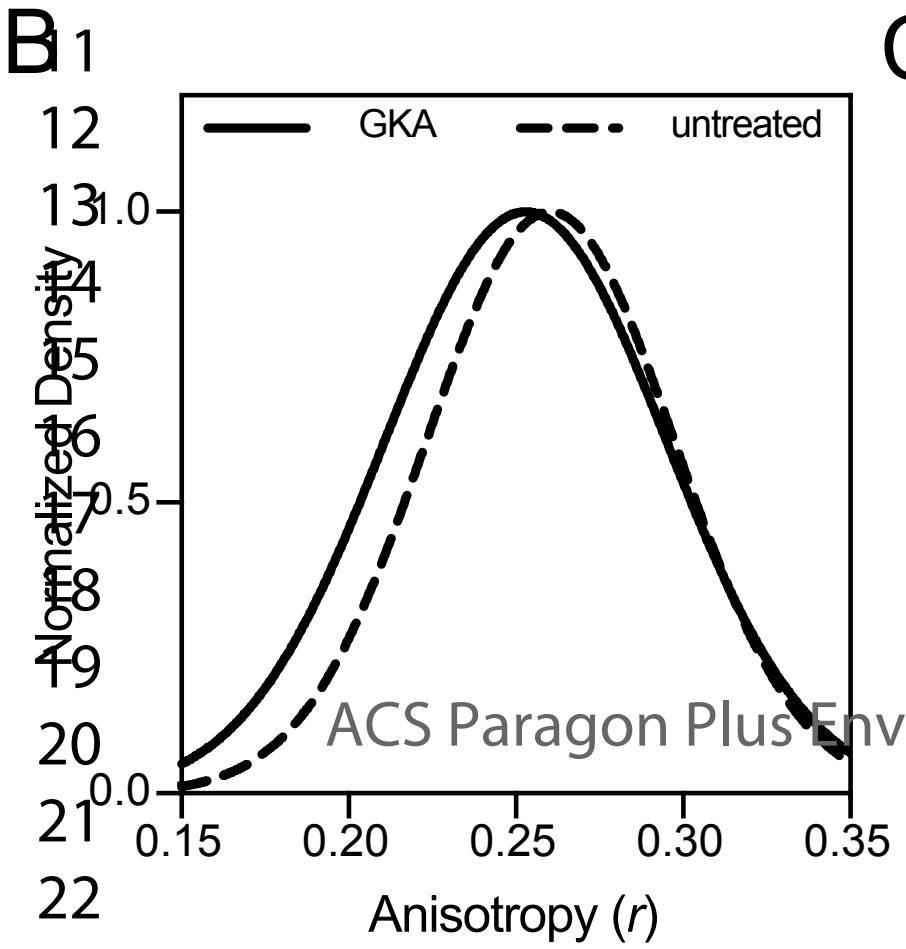

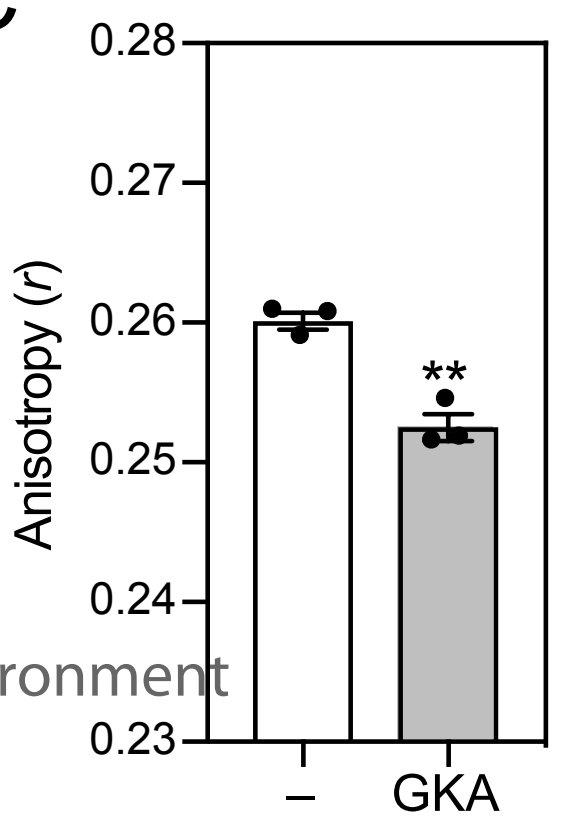

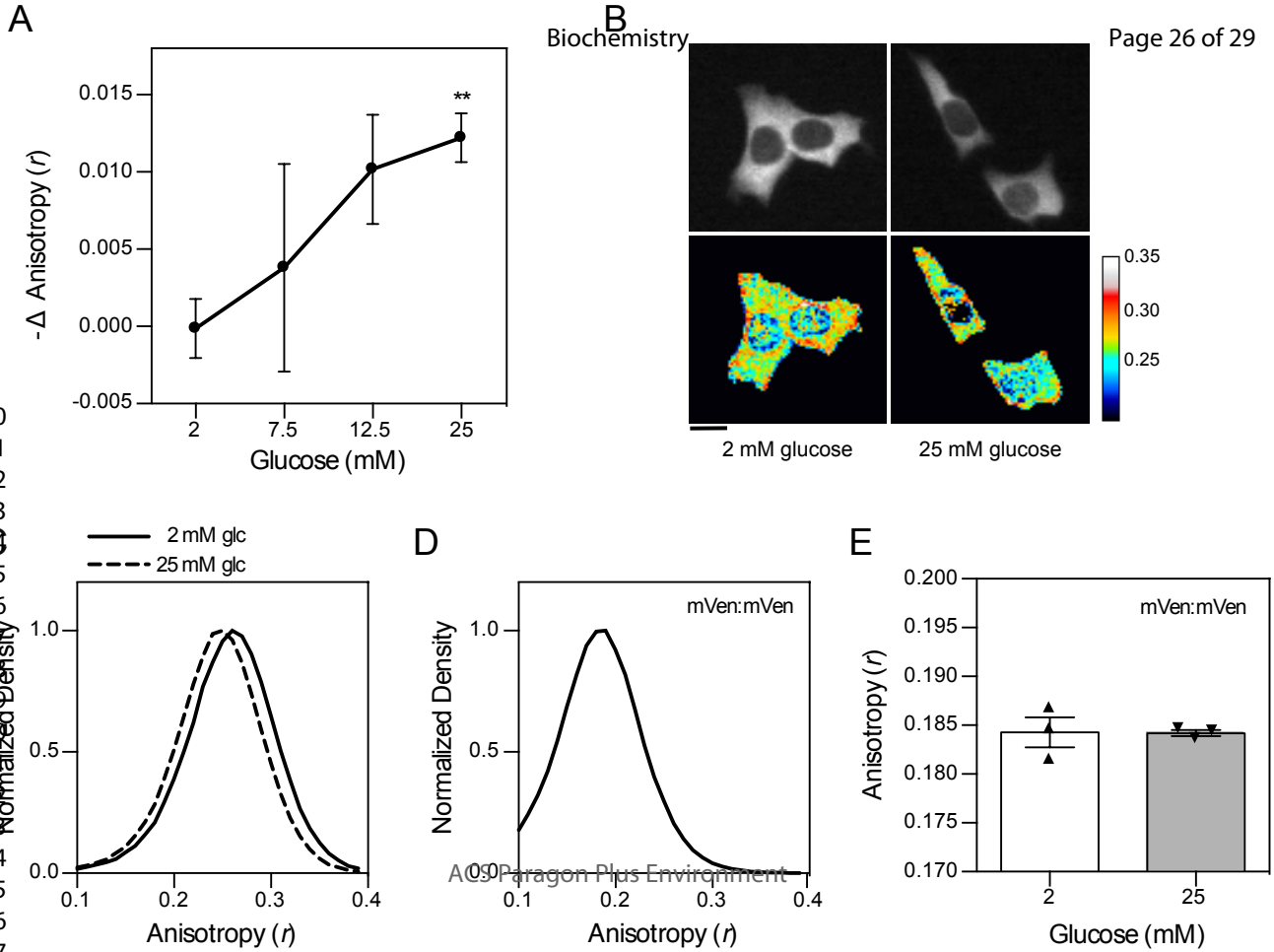

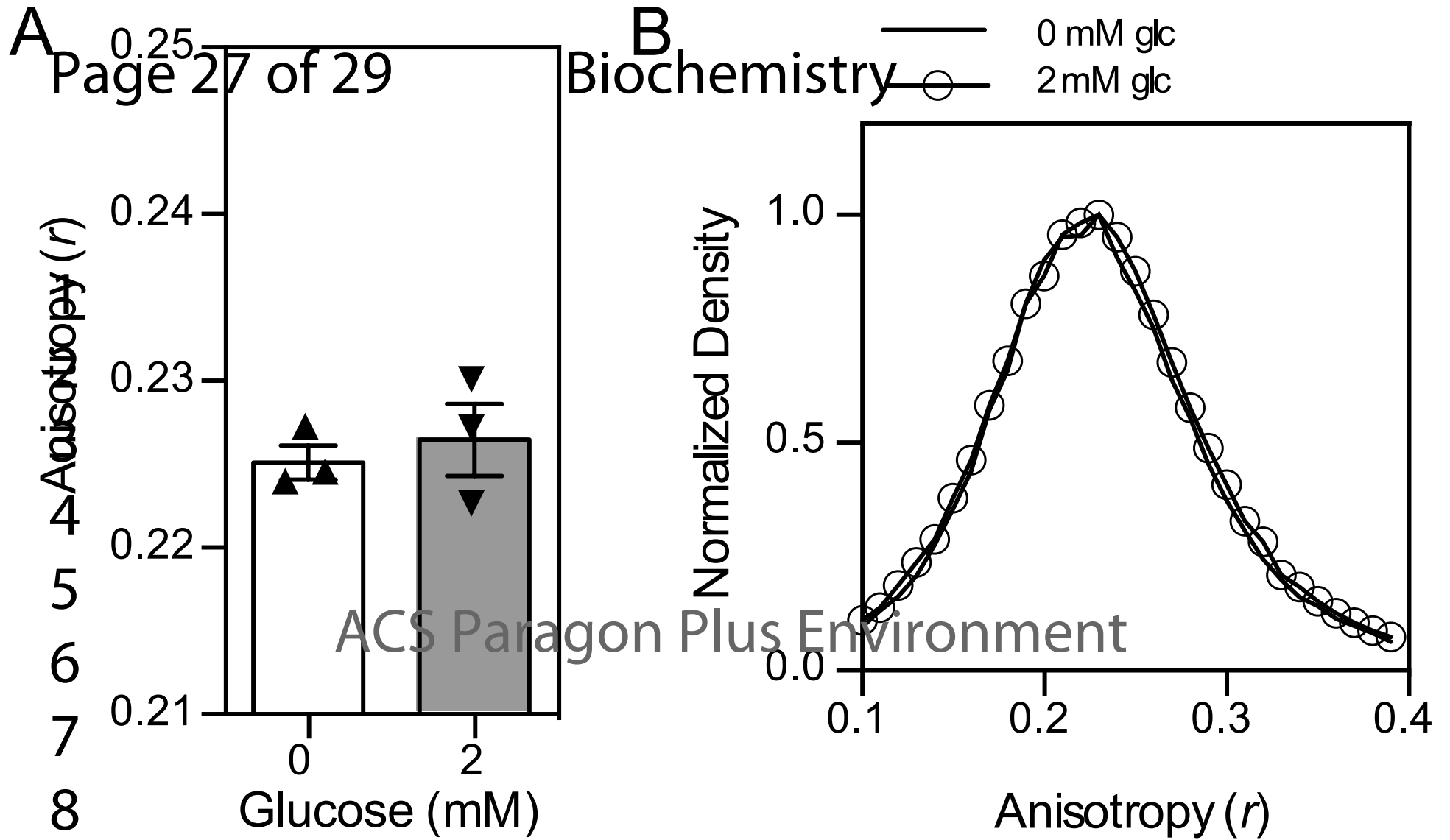

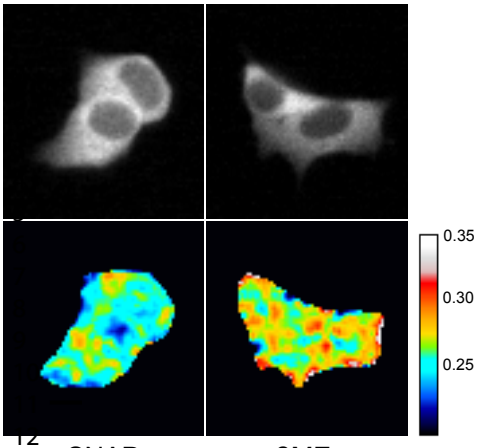

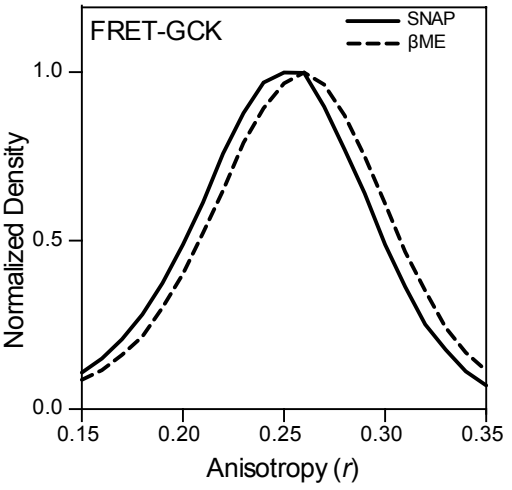

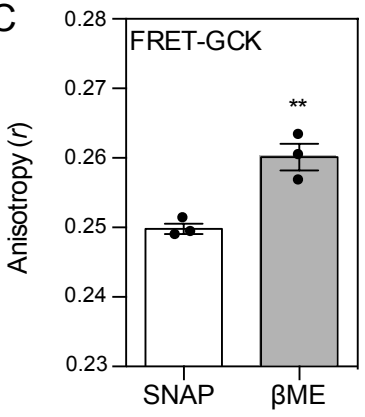

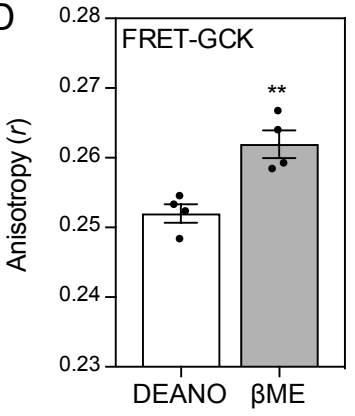

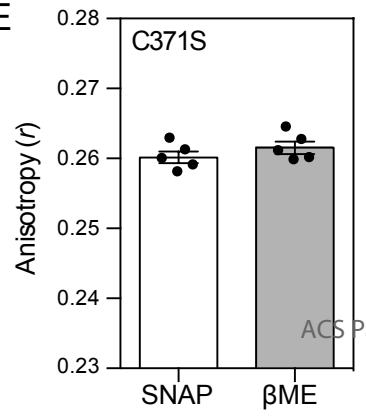

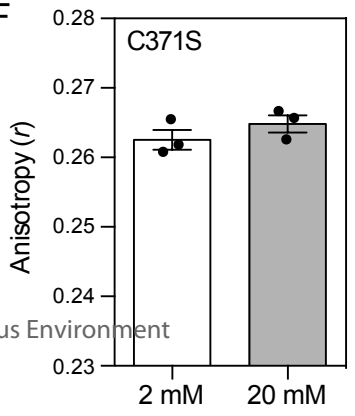

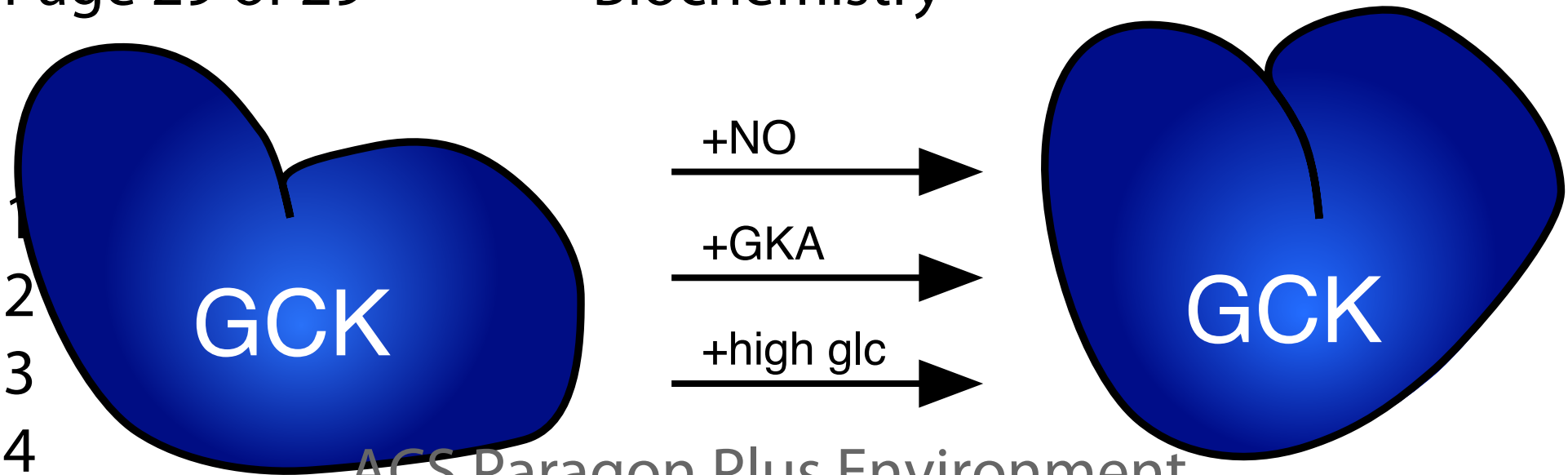

Low Activity

High Activity